# The Cutoff Region of a Rectangular Waveguide with Losses, Its Properties and Uses*

By L. U. KIBLER

(Manuscript received February 10, 1969)

*The effect of the wall and the dielectric losses on the operation of a rectangular waveguide at frequencies in the cutoff region was investigated both theoretically and experimentally. A new measurement technique that permits determining the electrical properties of metals and dielectrics at microwave frequencies was developed from these investigations.*

## I. INTRODUCTION

Physical waveguides have walls with finite conductivity and enclose dielectric regions that have finite losses. The usual high conductivity metals and low-loss dielectrics have little effect on wave propagation at frequencies well above and below the cutoff frequency region.† These metallic and dielectric losses, however, have a pronounced effect in a small frequency region that includes the nominal cutoff frequency for a particular mode as determined for a lossless waveguide of the same geometry.[1] The purpose of this paper is the theoretical and experimental investigation of the properties of a physical waveguide operated at frequencies in this latter region.

The scope of this investigation is limited to a rectangular waveguide operated in the 8.2 to 12.4 GHz band of frequency (X band). The dominant mode of the lossless waveguide, the $TE_{10}$ mode, serves as the initial model for an analysis of a similar mode configuration when losses are present. The analysis is divided into two parts: first, the waveguide is assumed to have two narrow walls with conductivity

* From the disertation submitted to the faculty of the Polytechnic Institute of Brooklyn in partial fulfillment of the requirements for the degree of Doctor of Philosophy (electrophysics), 1968.

† For a lossless waveguide, the cut frequency is a singular point for the propagation constant of a waveguide mode.

$\sigma_1$, and the two broad walls with conductivity $\sigma_2$; and second, the same waveguide is analyzed with a lossy dielectric slab centered between the narrow walls of the waveguide.

The results of this analysis are examined experimentally using waveguide sections that have several different wall conductivities. Additional experiments were conducted with two types of lossy dielectrics. The results of these experiments demonstrate the effect of wall losses and dielectric losses on propagation in the cutoff frequency region of the waveguide.

The major use motivating this study of the cutoff properties of a lossy waveguide is that of determining the electrical constants of metals and dielectrics. The conductivity of three metals, and the dielectric constant and loss tangent of two dielectrics are determined experimentally using the cutoff properties of the waveguide. Copper, nickel, and a nichrome-copper composite were chosen. The effect of a dc magnetic field on the conductivity of copper and nickel were also investigated. The magnetic field produced no measurable effect on copper; however, the apparent conductivity of nickel decreased. A tentative explanation of this observation is advanced. Lucite and micarta were chosen for the dielectric experiments.

Experimental values of these physical constants are determined to within an accuracy of less than 2 percent. Where published values of these constants are available, they are found to agree within a few percent with the electrical values we obtained. The difference between published values and the values determined by this cutoff measurement technique reflect the use of certain approximations in the analysis and the experiment errors. These two sources of error are not separable, but it is evident that they are quite small.

This experimental technique provides a marked departure from the classical resonant cavity techniques used in the past.[2] The chief advantage of the waveguide cutoff measurement technique lies in the ability to measure the properties of metals accurately at microwave frequencies. The properties of dielectrics can also be measured although the accuracy of the cutoff technique is about the same as that of the classical resonant cavity techniques. There remains, however, the general advantage of having alternate measurement techniques which may be more convenient in some instances.

## II. ANALYSIS

There are many analyses of the effects of losses in waveguides.[3-6] These efforts have been concerned with the effect of wall or dielectric

losses at frequencies well above or below the cutoff frequency of a particular mode. Barrow and Lender treated the effect of a finite wall conductivity on the propagation constant near the nominal cutoff of a circular waveguide.[7,8] Southworth noted that a decrease in the wall conductivity will decrease the frequency at which the cutoff region occurs.[9]

The classic method of treating wall losses and dielectric losses of a single mode in waveguides in the propagation region of the guide is to consider the power loss in the walls.[10] These approximate solutions are not valid in the vicinity of cutoff, since the lossless analysis on which they are based has a singularity at cutoff.

In order to accurately calculate the propagation constant of a waveguide with lossy walls and possibly containing a lossy dielectric, we must consider what field components must be present in the walls and in the dielectric. We will direct our attention to the $TE_{10}$ mode in the lossless waveguide as a starting point.

Refer to Fig. 1. The $TE_{10}$ mode in the lossless rectangular waveguide has the following field components; a $y$-directed electric field, a $z$-directed magnetic field and an $x$-directed magnetic field.

From these fields of the lossless waveguide, we can consider what other field components are necessary when the bounding walls have finite conductivity. At the side walls $x = 0$, $x = a$, there must be a $y$-directed electric field at the wall. On the top and bottom walls there must be an $x$-directed electric field and a $z$-directed electric field in the metal as a result of the finite currents in these directions. These fields must be supported by like directed fields in the dielectric region of the waveguide since the tangential electric and magnetic fields must be continuous across the dielectric-metal boundaries. Figure 1 shows the required field distributions.

In order to solve the field in the waveguide we must find a solution of Maxwell's equations for a possibly lossy dielectric surrounded by walls with finite conductivity. The finite conductive walls will be considered to be describable by their intrinsic impedance.

In a source free region, Maxwell's equations for a source free region with sinusoidal time dependence can be written for solution by vector potentials.[1] These vector potential equations became

$$\mathbf{E} = -\nabla \times \mathbf{F} - z\mathbf{A} + \frac{1}{y}\nabla(\nabla \cdot \mathbf{A}) \tag{1}$$

$$\mathbf{H} = \nabla \times \mathbf{A} - y\mathbf{F} + \frac{1}{z}\nabla(\nabla \cdot \mathbf{F}) \tag{2}$$

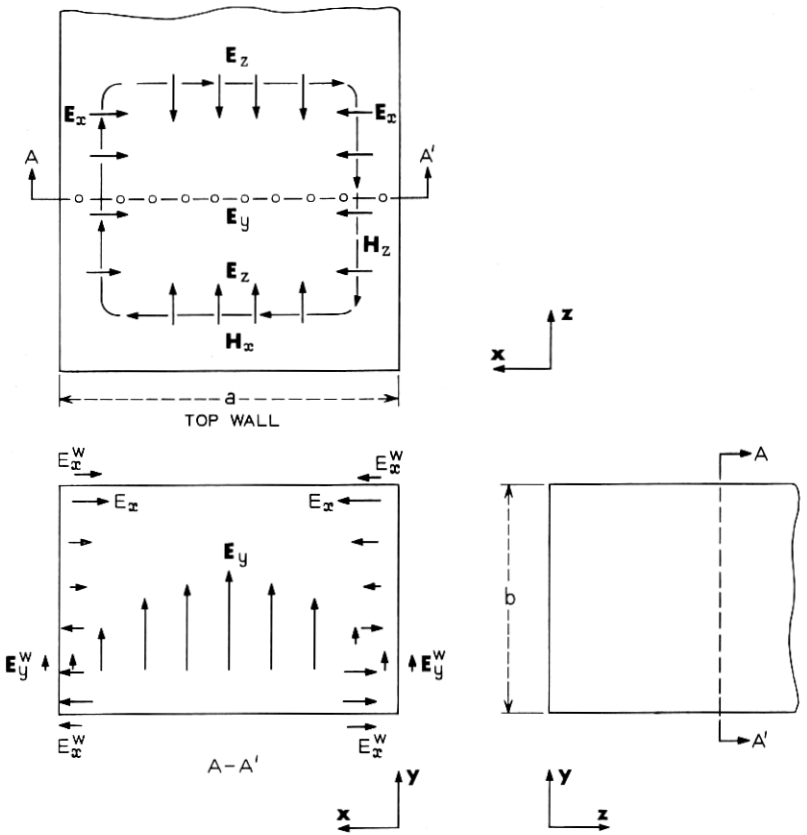


Fig. 1 — Field distribution of a lossy waveguide.

where $\mathbf{A}$ = magnetic vector potential
$\mathbf{F}$ = electric vector potential
$y(\omega) = \sigma + j\omega(\epsilon' - j\epsilon'')$ (admittance per unit length)
$z(\omega) = j\omega\mu$ (impedance per unit length)
$j = (-1)^{\frac{1}{2}}$

and

$\epsilon'$ = dielectric constant
$\epsilon''$ = dielectric loss factor
$\sigma$ = conductivity
$\mu$ = permeability.

The choice of a $y$-directed complex magnetic vector potential of the form

$$\mathbf{A} = \mathbf{u}_y A_m \sin K_{x_o} x \cos K_{y_o} y \exp(-\gamma z) \tag{3}$$

where $A_m$ is an arbitrary constant yields, after substitution in equations (1) and (2), the complex electric and magnetic field vectors in the dielectric region.

$$\mathbf{H}_x^e = A_m \gamma \sin K_{x_o} x \cos K_{y_o} y \exp(-\gamma z)\mathbf{u}_x \tag{4a}$$

$$\mathbf{H}_{z_o} = A_m K_{x_o} \cos K_{x_o} x \cos K_{y_o} y \exp(-\gamma z)\mathbf{u}_z \tag{4b}$$

$$\mathbf{E}_{x_o} = \frac{A_m K_{x_o} K_{y_o}}{y_o} \cos K_{x_o} x \sin K_{y_o} y \exp(-\gamma z)\mathbf{u}_x \tag{4c}$$

$$\mathbf{E}_{y_o} = \frac{A_m \sin K_{x_o} x \cos K_{y_o} y}{y_o} (k_o^2 - K_{y_o}^2) \exp(-\gamma z)\mathbf{u}_y \tag{4d}$$

$$\mathbf{E}_{z_o} = \frac{A_m K_{y_o} \gamma}{y_o} \sin K_{x_o} x \sin K_{y_o} y \mathbf{u}_z \tag{4e}$$

$$K_{x_o}^2 + K_{y_o}^2 - \gamma^2 = k_o^2 \tag{4f}$$

where

$$k_o^2 = -y_o z_o$$

and

$\gamma$ = complex longitudinal propagation constant
$K_{x_o}$, $K_{y_o}$ = complex transverse propagation constants.

In order to account for the properties of the metals that make up the waveguide walls, we define the surface impedance of a metal at microwave frequencies as

$$\left.\frac{E_y}{H_z}\right|_{\substack{x=a \\ x=o}} = Z(\text{side walls}) \equiv Z_s = R_s + jX_s$$

$$\left.\frac{E_x}{H_z}\right|_{\substack{y=b \\ y=o}} = Z(\text{top or bottom walls}) \equiv Z_T = R_T + jX_T \,. \tag{5}$$

In order to evaluate the surface impedance of the metal walls of the waveguide, we use the surface impedance for TEM waves in an unbounded lossy medium. This approximation is exact for a plane wave incident on a lossy metal. In the cutoff region the dominant mode fields can be approximately described by plane waves reflecting between the

side walls. Thus this definition of the surface impedance closely approximates the lossy waveguide in the cutoff region.

These wall impedances can be defined from $z(\omega)$ and $y(\omega)$ such that

$$Z_{S,T} = \text{Re}\left(\frac{z_{S,T}}{y_{S,T}}\right)^{\frac{1}{2}} + j\,IMAG\left(\frac{z_{S,T}}{y_{S,T}}\right)^{\frac{1}{2}}. \tag{6}$$

From (6) the intrinsic wall impedance for the conventional good conductors where $\sigma \gg \omega\epsilon$ can be obtained as

$$\begin{aligned} Z_S &= \left(\frac{\omega\mu_s}{2\sigma_s}\right)^{\frac{1}{2}}(1 + j) \\ Z_T &= \left(\frac{\omega\mu_T}{2\sigma_T}\right)^{\frac{1}{2}}(1 + j) \end{aligned} \tag{7}$$

The determination of the propagation constants $K_x$, $K_y$, and $\gamma$ results from application of the boundary conditions. These boundary conditions require continuity of the tangential $E$ and $H$ fields at each boundary. From equations (4) with conditions (5) and (7), we obtain

$$\frac{k_o^2 - K_{y_o}^2}{K_{x_o} y_o} \tan K_{x_o} a = \left(\frac{\omega\mu_s}{2\sigma_s}\right)^{\frac{1}{2}}(1 + j) \tag{8a}$$

$$\frac{K_{y_o}}{y_o} \tan K_{y_o} b = \left(\frac{\omega\mu_T}{2\sigma_T}\right)^{\frac{1}{2}}(1 + j). \tag{8b}$$

These equations (8) are transcendental and are solvable on a digital computer. Solution of (8b) for $K_{y_o}$ allows the solution of (8a) for $K_{x_o}$ for each frequency of interest. The $z$-directed propagation constant $\gamma$ can be determined by substituting $K_{x_o}$ and $K_{y_o}$ into (4f).

It is evident that a set of curves for $\gamma$ can be plotted for various values of $R_{S,T}$ and $X_{S,T}$. Thus from measured values of $\gamma$, the values of $R_{S,T}$ and $X_{S,T}$ can be determined, and hence the values of $\sigma_s$ or $\sigma_T$.

The solutions represented by equations (8) can be used to determine the characteristics of the cutoff region of waveguides that have walls made of composite or coated metals. The intrinsic impedance of such conductors has been solved by Ramo and Whinnery.[11] The solution is given below.

$$Z_{COMP} = R_1(1 + j)\left(\frac{\sinh \tau_1 d + \dfrac{R_2}{R_1}\cosh \tau_1 d}{\cosh \tau_1 d + \dfrac{R_2}{R_1}\sinh \tau_1 d}\right) \tag{9}$$

where

$d$ = thickness of coating metal

$$\tau_1 = (1 + j)(\pi f \mu_1 \sigma_1)^{\frac{1}{2}}$$

$$R_1 = \left(\frac{\pi f \mu_1}{\sigma_1}\right)^{\frac{1}{2}}$$

$$R_2 = \left(\frac{\pi f \mu_2}{\sigma_2}\right)^{\frac{1}{2}}$$

$\sigma_1$ = conductivity of coating metal

$\sigma_2$ = conductivity of coated metal

$\mu_1$ = permeability of coating metal

$\mu_2$ = permeability of coated metal.

$Z_{COMP}$ can be substituted for either $Z_S$ or $Z_T$ in equations (8) depending on which walls of the waveguide are coated.

The most general solution of a waveguide in the cutoff region must include not only the effects of walls with finite conductivity but also the effect of a lossy dielectric. When the dielectric completely fills the interior of the waveguide the solutions just given can be used by inserting the complex dielectric constant defined above.

Because of a limited physical size of the available dielectrics or to accommodate certain measurement techniques discussed later, it may be necessary to use a thin slab of dielectric material that only partially fills the interior of the waveguide. Figure 2 is a sketch of such a dielectric slab waveguide.

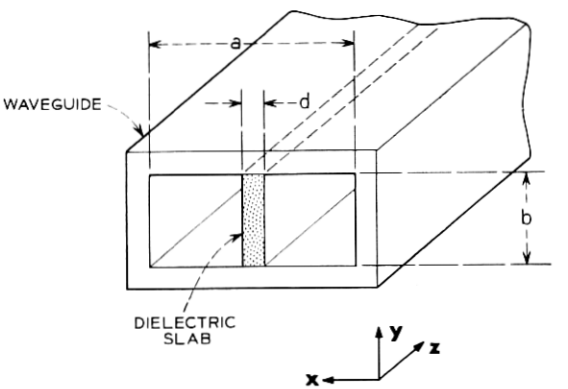


Fig. 2 — Dielectric slab waveguide.

The analysis of a lossy dielectric slab centered in a waveguide whose walls have finite conductivity proceeds from equations (1) and (2). The field solution if losses are assumed present only in the top and bottom walls can be obtained by choosing a $y$-directed complex electric vector potential

$$\mathbf{F} = \mathfrak{y}_y \varphi. \tag{10}$$

A solution which satisfies the physical requirements of the dielectric slab waveguide dominant mode can be obtained by choosing the $\varphi$'s as

$$\begin{aligned}
\varphi_d &= B_l \cos K_{xd}\left(x - \frac{a}{2}\right) \cos K_{yd} y \exp(-\gamma z) && \frac{a-d}{z} \leqq x \leqq \frac{a+d}{z} \\
\varphi_o &= A_l \sin K_{xo}(a - x) \cos K_{yo} y \exp(-\gamma z) && \frac{a+d}{2} \leqq x \leqq a \\
\varphi_o' &= A_l \sin K_{xo} x \cos K_{yo} y \exp(-\gamma z) && 0 \leqq x \leqq \frac{a-d}{z}
\end{aligned} \tag{11}$$

where $A_l$ and $B_l$ are arbitrary constants. The field components in the three regions of the dielectric slab waveguide are determined by substituting the electric vector potentials represented by (10) and (11) into the field equations (1) and (2).

In the dielectric region $(a - d)/2 \leqq x \leqq (a + d)/2$, the field components are

$$\begin{aligned}
\mathbf{E}_{yd} &= \gamma B_l \cos K_{xd}\left(x - \frac{a}{2}\right) \cos K_{yd} y \exp(-\gamma z)\mathfrak{y}_y \\
\mathbf{E}_{zd} &= -K_{yd} B_l \cos K_{xd}\left(x - \frac{a}{2}\right) \sin K_{yd} y \exp(-\gamma z)\mathfrak{y}_z \\
\mathbf{H}_{xd} &= \frac{(k_d^2 - K_{xd}^2)}{z_d} B_l \cos K_{xd}\left(x - \frac{a}{2}\right) \cos K_{yd} y \exp(-\gamma z)\mathfrak{y}_x \\
\mathbf{H}_{yd} &= \frac{B_l}{z_d} K_{xd} K_{yd} \sin K_{xd}\left(x - \frac{a}{2}\right) \sin K_{yd} y \exp(-\gamma z)\mathfrak{y}_y \\
\mathbf{H}_{zd} &= \frac{B_l \gamma K_{xd}}{z_d} \sin K_{xd}\left(x - \frac{a}{2}\right) \cos K_{yd} y \exp(-\gamma z)\mathfrak{y}_z
\end{aligned} \tag{12}$$

where

$\gamma$ = complex longitudinal propagation constant
$\gamma^2 = K_{xd}^2 + K_{yd}^2 - k_d^2$

$K_{xd}$ = $x$-directed propagation constant
$K_{yd}$ = $y$-directed propagation constant
$k_d^2$ = $\omega^2 \mu_d \epsilon_d$
$z_d$ = $j\omega\mu_d$
$a$ = guide width
$d$ = width of dielectric slab
$\mu_d$ = dielectric permeability
$\epsilon_d$ = $\epsilon_d' - j\epsilon_d''$
$\epsilon_d'$ = dielectric permitivity
$\epsilon_d''$ = dielectric loss factor.

In the region defined by $0 \leqq x \leqq (a - d)/2$ the field components become

$$\begin{aligned}
\mathbf{E}_{y_o}' &= \gamma A_l \sin K_{x_o} x \cos K_{y_o} y \exp(-\gamma z)\mathbf{u}_y \\
\mathbf{E}_{z_o}' &= -K_{y_o} A_l \sin K_{x_o} x \sin K_{y_o} y \exp(-\gamma z)\mathbf{u}_z \\
\mathbf{H}_{x_o}' &= \frac{(k_o^2 - K_{x_o}^2)}{z_o} A_l \sin K_{x_o} x \cos K_{y_o} y \exp(-\gamma z)\mathbf{u}_x \\
\mathbf{H}_{y_o}' &= \frac{A_l}{z_o} K_{x_o} \cos K_{x_o} x \sin K_{y_o} y \exp(-\gamma z)\mathbf{u}_y \\
\mathbf{H}_{z_o}' &= -\frac{A_l K_{x_o} \gamma}{z_o} \cos K_{x_o} x \cos K_{y_o} y \exp(-\gamma z)\mathbf{u}_z \,.
\end{aligned} \tag{13}$$

In the region defined by $[(a + d)/2] \leqq x \leqq a$ the field components are

$$\begin{aligned}
\mathbf{E}_{y_o} &= \gamma A_l \sin K_{x_o}(a - x) \cos K_{y_o} y \exp(-\gamma z)\mathbf{u}_y \\
\mathbf{E}_{z_o} &= -K_{y_o} A_l \sin K_{x_o}(a - x) \sin K_{y_o} y \exp(-\gamma z)\mathbf{u}_z \\
\mathbf{H}_{x_o} &= \frac{(k_o^2 - K_{x_o}^2)}{z_o} A_l \sin K_{x_o}(a - x) \cos K_{y_o} y \exp(-\gamma z)\mathbf{u}_x \\
\mathbf{H}_{y_o} &= \frac{A_l K_{x_o} K_{y_o}}{z_o} \cos K_{x_o}(a - x) \sin K_{y_o} y \exp(-\gamma z)\mathbf{u}_y \\
\mathbf{H}_{z_o} &= \frac{A_l K_{x_o} \gamma}{z_o} \cos K_{x_o}(a - x) \cos K_{y_o} y \exp(-\gamma z)\mathbf{u}_z
\end{aligned} \tag{14}$$

where

$\gamma$ = complex longitudinal propagation constant
$\gamma^2$ = $k_{x_o}^2 + K_{y_o}^2 - k_o^2$
$K_{x_o}$ = $x$-directed propagation constant
$K_{y_o}$ = $y$-directed propagation constant

$k_o^2 = \omega^2 \mu_o \epsilon_o$
$z_o = j\omega\mu_o$
$\mu_o$ = permeability of vacuum
$\epsilon_o$ = permitivity of vacuum.

The total field solution of the dielectric slab waveguide is obtained by matching the tangential electric and magnetic fields at the dielectric-air boundaries. Matching these field quantities yields

$$\frac{K_{xd}}{z_d} \tan K_{xd} \frac{d}{2} = \frac{K_{xo}}{z_o} \cot K_{xo}\left(\frac{a-d}{2}\right) \tag{15a}$$

$$\frac{z_d K_{yd}}{(k_d^2 - K_{xd}^2)} \tan K_{yd} b = Z_T \tag{15b}$$

$$\frac{z_o K_{yo}}{(k_o^2 - K_{xo}^2)} \tan K_{yo} b = Z_T \tag{15c}$$

where $Z_T$ is the surface impedance of the top and bottom walls of the waveguide.

Attempts to include the effects of the finite conductivity of the side walls in this solution were not successful. This failure stems from the lack of conformance of the boundary conditions and the coordinate surfaces. However, the fields in a waveguide operated in the cutoff region are approximately TEM waves in the transverse direction. We can use this fact to modify equations (15) to include the effects of the finite side wall conductivity. For this modifying solution we turn to a transverse resonance type of analysis.

Consider the dielectric slab waveguide in Fig. 2 at cutoff as a lossless parallel plate waveguide. The side wall of the waveguide is represented by its intrinsic admittance, $y_s$. The center of the guide is considered an open circuit. The admittance looking to the right, $y_1$, and to the left, $y_2$, of the dielectric-air boundary, is given by

$$\begin{aligned} y_1 &= y_o \frac{y_s + jy_o \tan K_{xo}\left(\frac{a-d}{2}\right)}{y_o + jy_s \tan K_{xo}\left(\frac{a-d}{2}\right)} \\ y_2 &= jy_d \tan K_{xd} \frac{d}{2} \end{aligned} \tag{16}$$

where

$$y_o = \left(\frac{\epsilon_o}{\mu_o}\right)^{\frac{1}{2}}$$

$$y_d = \left(\frac{\epsilon_d}{\mu_d}\right)^{\frac{1}{2}}$$

$$y_s = \frac{1}{z_s} = \frac{1}{\left(\frac{\omega\mu}{2\sigma_s}\right)^{\frac{1}{2}}(1 + j)}$$

$K_{x_d} = \omega_c(\mu_d\epsilon_d)^{\frac{1}{2}}$ at resonance
$K_{x_o} = \omega_c(\mu_o\epsilon_o)^{\frac{1}{2}}$ at resonance
$\omega_c$ = resonance or cutoff angular frequency.

The condition for resonance is then given by

$$y_1 = -y_2 . \tag{17}$$

Substitution of (16) into (17) yields

$$y_o\left[\frac{1 + jy_oz_s \tan K_{x_o}\left(\frac{a-d}{2}\right)}{y_oz_s + j \tan K_{x_o}\left(\frac{a-d}{2}\right)}\right] = -jy_d \tan K_{x_d}\frac{d}{2}. \tag{18}$$

Since $jy_oz_s$ will be a small value for practical wall metals, we can use the approximation

$$jy_oz_s = \alpha \approx \tan \alpha. \tag{19}$$

Equation (18) then becomes

$$-jy_o\left[\frac{1 + \tan\alpha \tan K_{x_o}\left(\frac{a-d}{2}\right)}{-\tan\alpha + \tan K_{x_o}\left(\frac{a-d}{2}\right)}\right] = -jy_d \tan K_{x_d}\frac{d}{2}. \tag{20}$$

The bracketed function on the left side of equation (20) is the expansion of $\cot(A\text{-}B)$; hence (20) becomes

$$y_o \cot\left[K_{x_o}\left(\frac{a-d}{2}\right) - jy_oz_s\right] = y_d \tan K_{x_d}\frac{d}{2}. \tag{21}$$

Equation (21) has the general trigonometric form of the field solution given in equation (15a). Substituting the values for $y_o$ and $y_d$ and multiplying and dividing by $K_{x_o}$ and $K_{x_d}$ yields when the common terms of $\mu_o$, $\epsilon_o$, $\epsilon_d$ and $\mu_d$ are cancelled and $K_{x_o}$ and $K_{x_d}$ are reintroduced and the

equation rearranged

$$\frac{K_{x_o}}{z_o} \cot \left[ K_{x_o} \left( \frac{a-d}{2} \right) + \frac{K_{x_o} z_s}{z_o} \right] = \frac{K_{x_d}}{z_d} \tan K_{x_d} \frac{d}{2}. \tag{22}$$

Equation (22) is the same form as equation (15a) except for the modification of the argument of the cotangent function by the effect of the side wall impedance. Because of the evident similarity of equations (15a) and (22), we can interpret $K_{x_o}$ as the transverse complex propagation constant that is valid not only at cutoff but over a range of frequencies extending on either side of cutoff.

The term $z_s/z_o$ can be expanded by using the definition of the skin depth, $\delta$

$$\delta = \left( \frac{2}{\omega \mu \sigma} \right)^{\frac{1}{2}} \tag{23}$$

to yield

$$\frac{z_s}{z_o} = \frac{(1-j)\delta}{2}. \tag{24}$$

The argument of the cotangent term becomes

$$K_{x_o} \left[ \frac{a-d}{2} + \frac{(1-j)\delta}{2} \right]. \tag{25}$$

Argument (25) indicates that the width of the air region of the dielectric-slab waveguide is increased by an amount proportional to the skin depth. A similar result was obtained by Adler, Chu, and Fano, who analyzed the minimum of the standing wave pattern for a plane wave at an air-lossy metal interface.[12]

The equations which furnish the solution of a lossy dielectric slab centered in a waveguide with lossy walls in the region of cutoff are given by

$$\frac{K_{x_o}}{z_o} \cot K_{x_o} \left[ \frac{(a-d)}{2} + \frac{(1-j)\delta}{2} \right] = \frac{K_{x_d}}{z_d} \tan K_{x_d} \frac{d}{2} \tag{26a}$$

$$\frac{z_d K_{y_d} \tan K_{y_d} b}{[k_d^2 - K_{x_d}^2]} = Z_T \tag{26a}$$

$$\frac{z_o K_{y_o} \tan K_{y_o} b}{[k_o^2 - K_{x_o}^2]} = Z_T \tag{26c}$$

$$\gamma^2 = K_{x_o}^2 + K_{y_o}^2 - k_o^2 \tag{26d}$$

$$\gamma^2 = K_{x_d}^2 + K_{y_d}^2 - k_d^2 . \tag{26e}$$

These are complex transcendental equations and were solved by a digital computer.

Equations (26), which provide the solution for the propagation constant of a lossy waveguide with a centered lossy dielectric slab operated in the cutoff region, were derived using several approximations. These approximations are considered quite accurate for frequencies in the cutoff region. At frequencies outside the cutoff region, these approximations lead to an increasing error in the computation of the longitudinal propagation constant. Thus, the electrical properties of materials cannot be determined accurately for frequencies outside the cutoff region. The accuracy of the measurements in the cutoff region will be evident from the experimental results.

## III. EXPERIMENTAL CIRCUITS

The analysis in Section II shows that the cutoff region of a waveguide with losses in the walls and dielectric is basically characterized by the complex longitudinal propagation constant. The other descriptive parameters such as impedance, admittance, scattering coefficients, and so on, depend on this propagation constant.

The propagation constant can be measured experimentally by determining the total attenuation and the total phase shift of a section of uniform waveguide whose length is known accurately. Accurate measurement of either attenuation or phase shift is difficult to obtain. However, differences in phase shift and in attenuation can be measured with great accuracy.

The experimental circuit was designed to measure differences in attenuation and phase shift. Figure 3 shows the basic experimental circuit. It is a microwave form of the usual low frequency comparison circuit. A common source supplies two paths. The path B is used as a reference path. Path A, the comparison path, has two separate test paths, $A_1$ and $A_2$, either of which may be chosen by proper positioning of the waveguide switches 1 and 2. The two main circuit paths are connected to a phase detector and to an amplitude detector by positioning switches 3 and 4.

These experiments could be conducted at any number of microwave frequencies. Available tables of the properties of metals and dielectrics show that these materials have a marked change in their dc properties in the X band of frequencies.[11,13] For this reason and the availability of accurate test equipment, the center of the X band of frequencies, about 9.5 GHz, was chosen for the design of the experimental circuit.

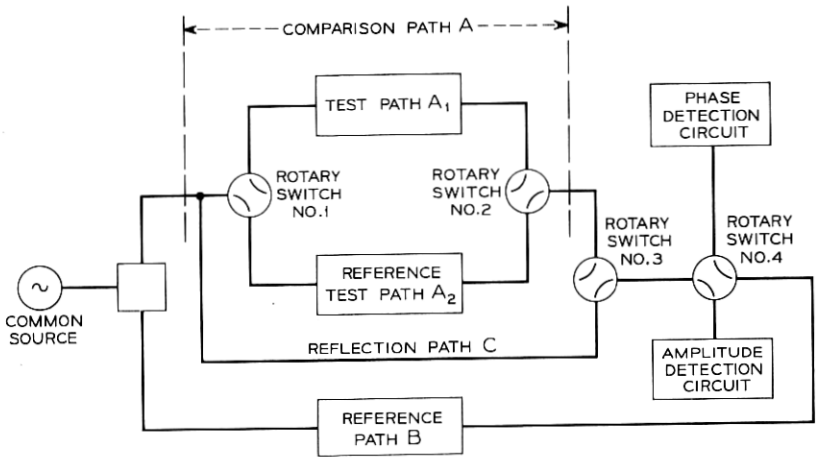


Fig. 3 — Simplified schematic diagram of experimental circuit.

The complete experimental circuit is shown schematically in Fig. 4. Standard commercial precision waveguide components were used throughout. Isolators were chosen to have voltage standing wave ratio's of less than 1.08 and isolation greater than 40 dB. The phase detection circuit was the kind described by Cohn.[14] It can measure phase differences to an accuracy of 0.05°. The amplitude detection circuit was used in conjunction with the tandem precision rotary vane attenuators (path A, Fig. 4). This combination was capable of measuring attenuation differences to an accuracy of 0.005 dB.

A precision rotary vane phase shifter was calibrated against the phase detection circuit and both were calibrated with selected lengths of precision X band waveguide. The phase shifter (path B, Fig. 4) and the phase detection circuit were used in combination for phase difference measurements.

Two types of waveguide test sections (see Fig. 5) were designed for use in these studies of the properties of a waveguide operated at cutoff. We designate these as a type A and a type B test section. Both types were electroformed of oxygen-free hard copper. Mandrels of the required dimensions for each test section were machined from aluminum, and polished to remove any roughness. The wall thickness of both types of test sections was a nominal $\frac{9}{16}$ inch.

Each type A test section was electroformed in one piece. Standard X-band flanges, type UG-39/1, were soldered to each end of a test

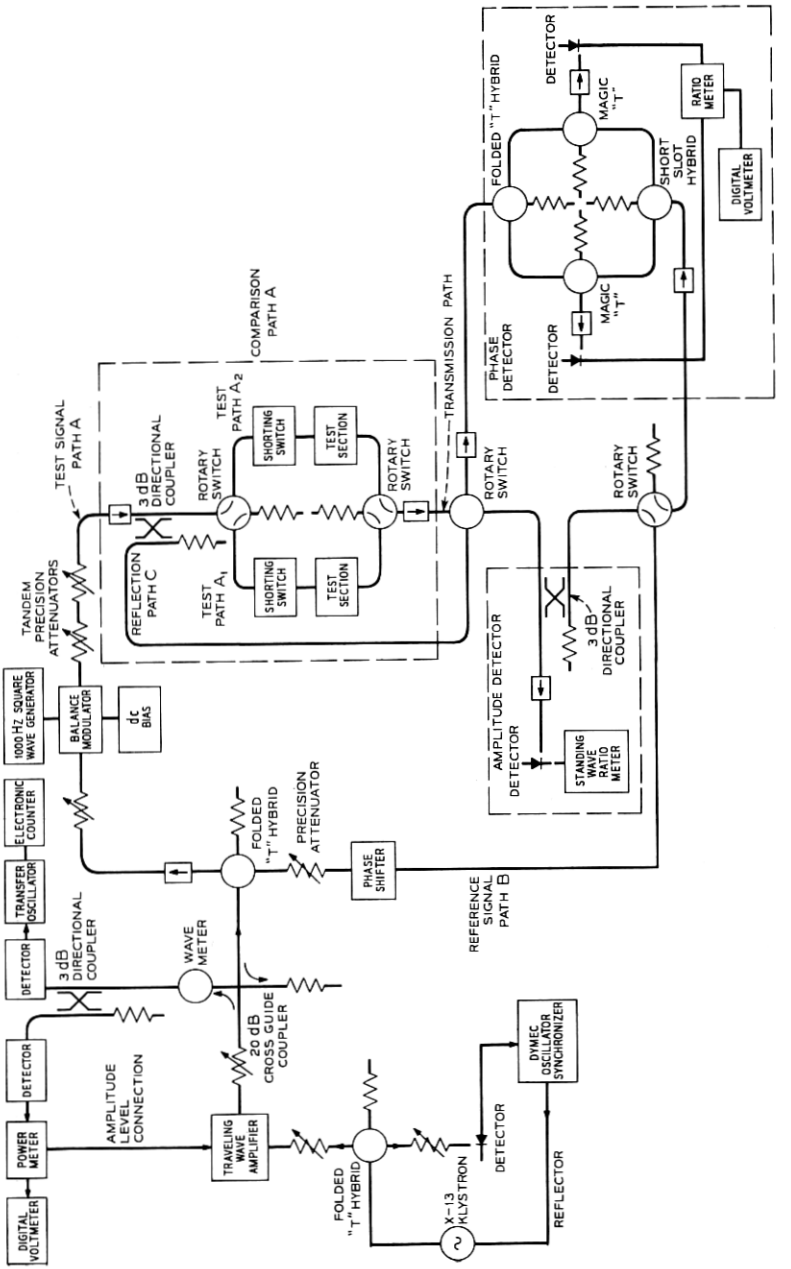


Fig. 4 — Experimental circuit for cutoff waveguide measurement.

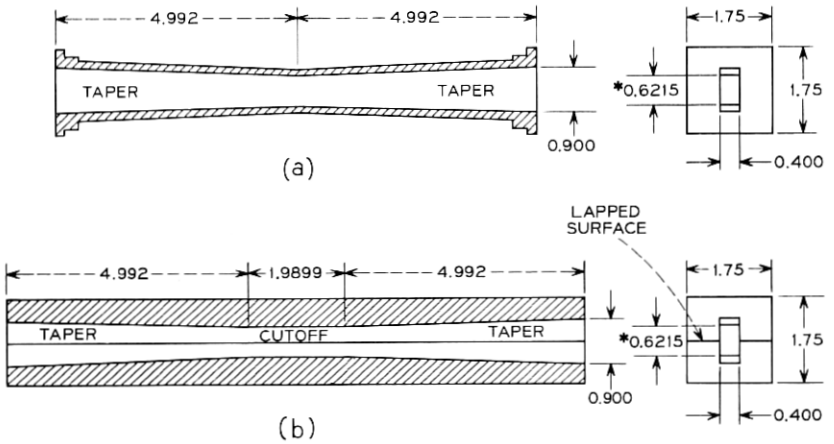


Fig. 5 — (a) Type A and (b) type B waveguide test sections. Dimensions are in inches. * The widths of the test sections were measured with gauge blocks to insure accuracy.

section. The flanges were machined and lapped to a smooth mating surface. Two alignment pins were inserted in each flange. Figure 6 shows a complete type A section.

The type B test sections were made in two halves (see Fig. 7). These halves were joined along the center of the broad faces of the waveguide walls. Each half of the type B test section was mounted in a brass channel for rigid support. The joining faces of these brass mounting channels were polished to achieve the required width. Alignment pins assured accurate assembly of the two halves. The joining surfaces were machined and lapped for accurate mating. The halves were held

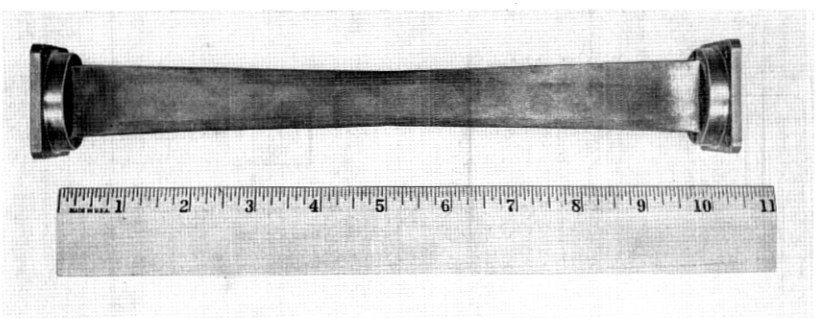


Fig. 6 — A complete type A waveguide test section.

together by 24 10-32 bolts. Threaded holes to mate standard X-band flanges were placed in each end of the type B test section. A dielectric slab is shown inserted in one half.

The type B test sections were used to examine the conductivity of various metals. These metals were placed on the walls of the cutoff portion of the type B sections by plating or evaporation. These test sections were made in halves for two reasons. First, it was possible to obtain uniform metal deposit on the three walls of the channel that results from making the section in halves. Uniform metal deposits on the interior walls of a closed test section was difficult if not impossible. Second, when metal is deposited on the walls of a waveguide, the interior dimensions are reduced by the metal thickness. At cut-

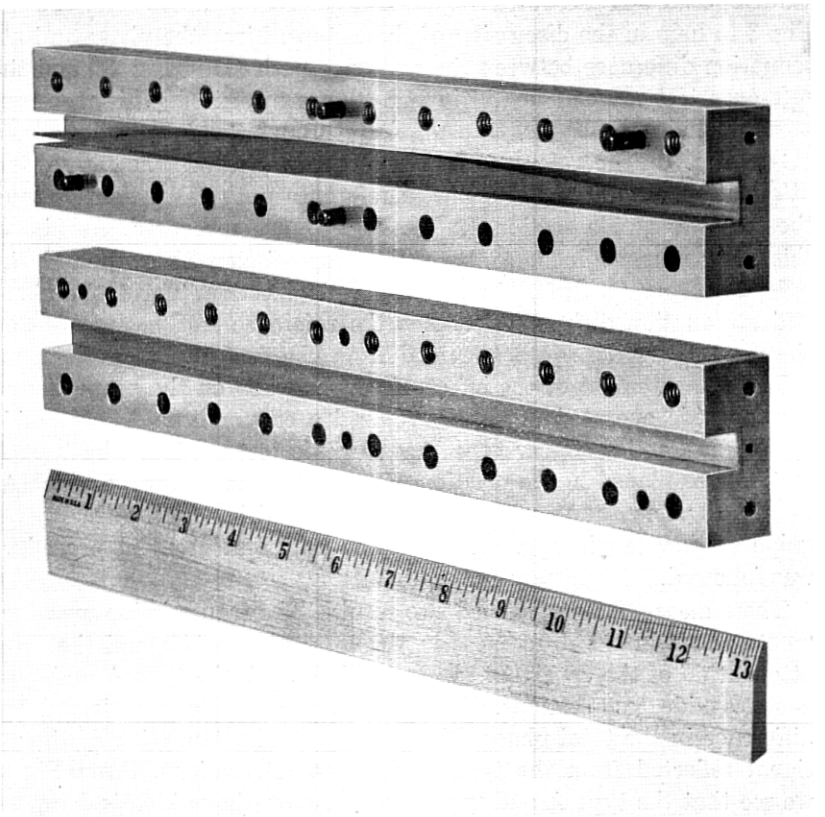


Fig. 7 — Type B waveguide test section with a dielectric slab in the top half.

off these small changes (0.0001 inch or less) in the waveguide height are insignificant. However, the same magnitude of dimension change in the width are very significant. By using two halves and by depositing the same thickness of metal on the joining surfaces as on the walls, there is an automatic compensation of the width change. The metal deposited on the narrow walls decreases the waveguide width, but the metal deposited on the joining surfaces increases the width on joining the halves by the same amount. Thus, the waveguide width was kept constant regardless of the thickness of the deposited metal.

## IV. EXPERIMENTAL MEASUREMENT PROCEDURE

The general procedure for measuring the properties of a waveguide operated in the cutoff region is divided into three steps. We use Fig. 3 to help in the discussion of these steps. First, the phase and attenuation difference between the reference path (B in Fig. 3) and the reference test waveguide ($A_2$ in Fig. 3) are measured. This measurement includes both the transmission through, and reflection from (C in Fig. 3) the reference test waveguide. Second, the phase and attenuation difference between the reference path (B in Fig. 3) and the test waveguide section ($A_1$ in Fig. 3) are measured. As above, this measurement includes both the transmission through and the reflection from (path C) the test waveguide section. Third, the phase and attenuation difference between the reference test waveguide and the test waveguide are determined from the first two measurements.

The measurement of the effect of copper walls on the properties of a waveguide operated at cutoff required a copper type A waveguide test section and a copper type B waveguide test section. The type A section was placed in the position of the reference test waveguide ($A_2$ in Fig. 3); and the type B section in the position of the test waveguide section ($A_1$ in Fig. 3). The three part measurement procedure was followed.

These measurements yielded two results. The transmission measurements result in the differences in the total phase shift and the total attenuation of the cw signal transmitted through the type A and type B waveguide test sections. The reflection measurements yielded the difference in the total phase shift and the total attenuation of the cw signal reflected from the type A and type B sections. From Fig. 5 we see that the type A and type B test sections have identical tapers. These tapers were adjusted to be electrically equal. The total phase shift and attenuation differences thus became the phase shift and at-

tenuation of the transmission through and the reflection from the 2-inch-long cutoff section contained in the type B test section.

The measurement of the effect of the dielectric slabs of lucite and micarta on the properties of the waveguide at cutoff followed the same procedure. The dielectric slabs (see Fig. 8) were centered in the type A and type B copper test sections. Since the tapers at the ends of the dielectric slabs are identical, the result of the measurement is the phase shift and the attenuation of the transmission through, and the reflection from, the dielectric loaded cutoff section of the type B test section.

The measurement of the effect of the other metallic walls, nickel and nichrome-copper, required only type B test sections. A copper type B test section was placed in the reference test waveguide position ($A_2$ in Fig. 3). An identical second copper type B test section was placed in the test section position ($A_1$ in Fig. 3). The electrical difference between these two test sections was determined for use in correcting future measurements.

The type B test section ($A_1$ in Fig. 3) was removed and the metals, nickel or nichrome, were applied over the copper walls of the cutoff region. The type B section was then reinserted into test position $A_1$. The measurement steps just described were repeated. The results of these measurements after correction for the possible electrical difference yielded the phase shift and attenuation of the signal transmitted through and reflected from the 2-inch long cutoff section of the type B waveguide section. The properties of the waveguide with nickel or nichrome walls operated in the cutoff region are determined from these results.

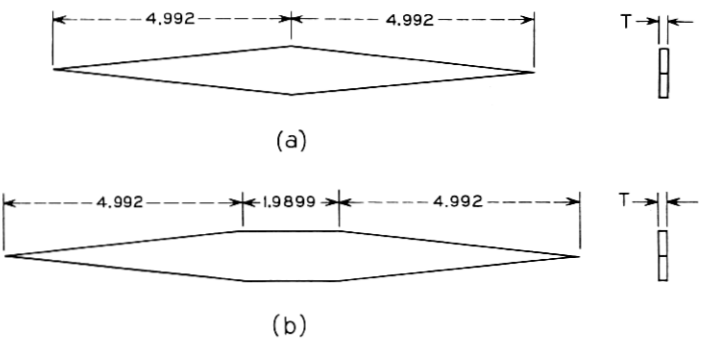


Fig. 8 — Dielectric slabs for (a) type A and (b) type B test sections. Dimensions are in inches.

These phase and attenuation measurements are used to calculate the complex propagation constant of a waveguide operated at frequencies in the cutoff region. These calculations are based on an analysis developed by Southworth (see pp. 57 and 58 of Ref. 9). He defines a voltage wave progressing down a finite length transmission line and suffering repeated reflections from mismatches at the input and output of the line. Southworth derives an expression for the steady state voltage at any point on the line. Using Southworth's notation we define $V_l$ as the voltage transmitted to the output of the cutoff section and $V_0$ as the voltage reflected to the input of the cutoff section. The difference between these two "voltages" can be written using Southworth's results as

$$(V_l - V_0) = [\exp(-\gamma_0 l) - 1]. \tag{27}$$

The measurement of $(V_l - V_0)$ yields from (27), the experimental value of $\gamma_0$, the complex propagation of the cutoff region of the waveguide section.

The experimental measurements given by the phase shifter, the phase detection circuit, and the tandem attenuators were used to determine the value of $(V_l - V_0)$. Figures 3 and 4 should help in the following discussion. For the measurement of copper and dielectrics we have a type A test section in path $A_2$ and a type B test section in path $A_1$ of the comparison path A. We consider two voltage waves, $E_0$ and $E_1$. $E_0$ propagates in the comparison path A, and $E_1$ in the reference path B.

The attenuation and phase shift of test path $A_2$ from the input rotary switch to the center of the type A test section is defined as $A_0 \exp(j\Phi_0)$, and from the center of the type A test section to the output rotary switch as $B_0 \exp(j\Phi_1)$. The attenuation and phase shift of test path $A_1$ from the input rotary switch to the junction of the type B section taper and the cutoff section is defined as $A_0^1 \exp(j\Phi_0^1)$, and from the output of the cutoff section to the output rotary switch, $E_0^1 \exp(j\Phi_1^1)$. The voltage wave in the reference path B is defined as $E_1 \exp(j\theta_1)$.

Test path $A_2$ with a type A section inserted is connected to the comparison path. With the tandem attenuators set at an arbitrary value, the phase shifter is adjusted to provide a 45° phase difference between the comparison and reference paths. The outputs of the phase measuring circuit and the amplitude measuring circuit are proportional to

$$\Phi_0 + \Phi_1 = \theta_1 \pm 45° \tag{28a}$$

and

$$E_0A_0B_0 = M_0 = \text{SWR meter reading,} \tag{28b}$$

respectively.

When the comparison path is connected to test path $A_1$ with a type B test section inserted, the outputs of the phase measuring circuit and the amplitude measuring circuit are proportional to $\Phi_0^1 + \Phi_1^1 + \measuredangle V_l$ and $E_0A_0^1B_0^1 \mid V_l \mid$, respectively.

The tandem attenuators and the phase shifter are adjusted to return the outputs of the amplitude measuring circuit and the phase measuring circuit to their values when test path $A_2$ was connected to the comparison path. This condition is expressed as

$$\Phi_0^1 + \Phi_1^1 + \measuredangle V_l = \theta_1 + \theta_p \pm 45° \tag{29a}$$

$$T_1E_0A_0^1B_0^1 \mid V_l \mid = M_0 \tag{29b}$$

where $\theta_p$ is the change in the phase shifter and $T_1$, the change in the attenuators' reading.

The same analysis is applied to the voltage waves reflected from test paths A and B. The reflection from test path B is expressed as

$$2\Phi_0 = \theta_1 \pm 45° \tag{30a}$$

$$E_02A_0 = M_1 . \tag{30b}$$

The reflection from test path A is expressed as

$$2\Phi_0^1 + \measuredangle V_0 = \theta_1 + \theta_p^1 \pm 45° \tag{31a}$$

$$T_2E_02A_0^1 \mid V_0 \mid = M_1 \tag{31b}$$

where $\theta_p^1$ is the change in the phase shifter and $T_2$ is the change in the attenuators' reading.

Subtracting equation (28) from (29) yields

$$\Phi_0^1 - \Phi_0 + \Phi_1^1 - \Phi_1 + \measuredangle V_l = \theta_p \tag{32a}$$

$$T_1A_0^1B_0^1 \mid V_l \mid = A_0B_0 . \tag{32b}$$

A calibration procedure determines the difference between $\Phi_0$ and $\Phi_0^1$, and $\Phi_1$ and $\Phi_1^1$, and the ratio of $A_0^1/A_0$ and $B_0^1/B_0$. With these measured differences, $V_l$ is determined from the phase shifter change, $\theta_p$ in degrees, and the tandem attenuators' change, $T_1$ in dB.

Subtracting equation (30) from (31) yields

$$\measuredangle V_0 + 2\Phi_0^1 - 2\Phi_0 = \theta_p^1 \tag{33a}$$

$$T_2 A_0^1 \mid V_0 \mid = A_0 . \tag{33b}$$

Again the calibration procedure furnished the values of $\Phi_0^1 - \Phi_0$ and $A_0^1/A_0$. The value of $V_0$ was determined from the phase shifter change $\theta_p^1$ and the tandem attenuators' change $T_2$. The value of $V_l - V_0$ is determined by the phase shifter's and attenuators' change in reading. The value of $\gamma_0$ is calculated from these experimental measurements by equation (27).

This analysis is also applicable to measurements with type B test sections in both the reference test path and the test path as required for measurement of nickel and nichrome. We define the propagation constant for one type B test section cutoff region (copper) as $\gamma_0$ and for the second type B test section (nickel or nichrome) as $\gamma_1$. We can then write for the nickel or nichrome section

$$(V_l - V_0)_A = [\exp(-\gamma_{1l}) - 1] \tag{34a}$$

and for the copper section

$$(V_l - V_0)_{cu} = [\exp(-\gamma_0 l) - 1]. \tag{34b}$$

The difference of these two equations yield

$$\begin{aligned} \Delta_{A-cu} &= (V_l - V_0)_A - (V_l - V_0)_{cu} \\ &= [\exp(-\gamma_1 l) - \exp(-\gamma_0 l)]. \end{aligned} \tag{35}$$

This difference represents the measured difference between a copper type B test section and a type B test section with a nickel or nichrome cutoff section. The analysis used previously to describe the copper cutoff section measurements is applicable here to show that $\Delta_{A-cu}$ was evaluated by this measurement and $\gamma_0$ by the copper test section measurement; thus the value of $\gamma_1$ is determined.

Since nickel is a magnetic material, measurements were made on the nickel plated type B test section with a magnetic field applied. These measurements demonstrated qualitatively that this measuring technique could be used to detect the magnetic induced changes in conductivity of certain metals.

The magnetic field was obtained from a surplus horseshoe shaped magnetron magnet. The width of the pole pieces was approximately two inches and the gap approximately two and one quarter inches. The measured field between the poles was approximately 2100 gauss. The magnet was oriented with the type B test section to produce a magnetic field parallel to the electromagnetic field lines in the side walls of the waveguide. Because of its construction (horseshoe

shape), this magnet produced a nonuniform magnetic field in the waveguide walls. Uniform magnetic field sources were not available; hence, these experiments were qualitative.

Measurements were made with nichrome to determine the effect on the waveguide cutoff properties of a lossy metal. A second type B test section was inserted in test path $A_1$ in place of the nickel plated test section. The reference type B test section remained in test path $A_2$. The phase shift difference and the attenuation difference between test path $A_1$ and test path $A_2$ was measured for both transmitted and reflected signals. This was done to establish a reference for the type B test section in test path A.

The type B test section was removed from test path $A_1$ and disassembled. The two halves of the test section were masked and nichrome was vacuum evaporated on the two narrow sidewalls to a thickness of 800Å. The two halves were reassembled and the nichrome type B test section reinserted in its original position in test path $A_1$.

The properties of a waveguide partially loaded with a dielectric was examined in the cutoff frequency region. Two types of dielectrics were used, one with low loss, lucite; and one with moderate loss, micarta.* In addition to demonstrating the effects of dielectric at cutoff, the dielectric constant and the loss tangent were determined from these measurements. Figure 8 is a diagram of the dielectric slabs.

## V. EXPERIMENTAL RESULTS

In order to place the results of the experiments in the proper perspective, we note that the nominal cutoff frequency of a lossless waveguide 0.62150-inch wide operated in the dominant mode is 9502.030 MHz.

### 5.1 *Metallic Test Sections*

The general effect of decreasing the conductivity of the waveguide walls for frequencies in and near the cutoff region can be seen in Fig. 9. The conductivity ranges from the dc value of oxygen-free hard electroformed copper, $5.8 \times 10^5$ mho/cm (reciprocal ohms per centimeter), to approximately one tenth the conductivity of copper. At a single frequency, as the conductivity is decreased, the imaginary part of the propagation constant, $\beta$, increases. The real part of the propagation constant, $\alpha$, decreases with decreasing conductivity for fre-

* The micarta used was made of woven cotten impregnated with cresylic acid formaldehyde resin.

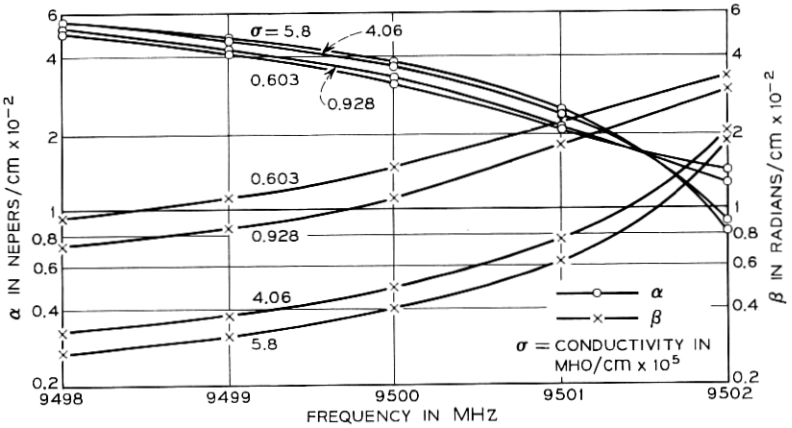


Fig. 9 — Propagation constant in cutoff region as a function of conductivity. $\gamma = \alpha + j\beta$.

quencies just below cutoff, but $\alpha$ increases for frequencies just above cutoff.

It is interesting that in Fig. 9 there is one frequency in the cutoff region for each value of conductivity where the real part of the propagation constant ($\alpha$) in nepers per centimeter equals the imaginary part of the propagation constant ($\beta$) in radians per centimeter. This frequency is properly defined as the cutoff frequency when the waveguide has walls with finite conductivity. Further examination of Fig. 9 shows that this defined cutoff frequency shifts to a lower frequency as the conductivity of the waveguide walls is decreased. We see that a decrease in conductivity by a factor of ten causes this defined cutoff frequency to shift by 850 KHz. Since microwave frequencies in this frequency region can now be measured to 1 KHz, the potential accuracy obtained by using this frequency shift for the measurement of the conductivity of metals is less than 1 per cent.

### 5.1.1 *Copper Test Sections*

The copper test section was measured at two different frequencies in the cutoff region. These frequencies, 9500.873 and 9497.960 MHz, were chosen to cover a region where Fig. 9 shows a maximum difference in $\alpha$ and $\beta$ for the range of expected copper conductivity. The calculated values of $\gamma l$ ($l$ in cm) for the first test frequency are plotted in Fig. 10 as a function of the conductivity (in mho/cm.) The value of $\gamma l$ was used instead of $\gamma$ to make comparison with the measured values easier, since

the measurement involves the total length of the test section and since the experimental errors are in dB and degrees. Each figure contains two curves; one for the total attenuation in dB, and one for the total phase shift in degrees.

The experimental values are plotted as points marked $\alpha_M$ and $\beta_M$ on the figure. The vertical broken lines with markings $\Delta\alpha$ and $\Delta\beta$ indicate the error limits in the experimental measurements. In Fig. 10, the error limits are smaller for the $\beta_M$ measured value than for the $\alpha_M$ value. The results at the second frequency, although not plotted, support the plotted results.

The average value of the conductivity of copper based on the $\alpha_M$

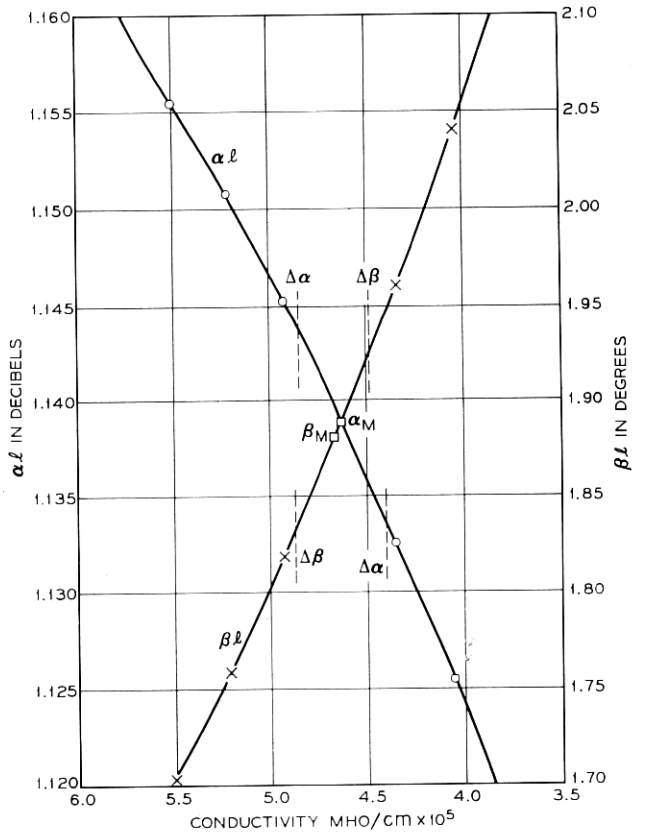


Fig. 10 — Copper experimental results at 9500.873 MHz yielding experimental value of conductivity. ○ calculated $\alpha l$, × calculated $\beta l$, and □ measured values.

measurement at the two frequencies is $4.635 \times 10^5$ mho/cm. The average value of the $\beta_M$ values is $4.685 \times 10^5$ mho/cm. The average of the mean of the maximum and minimum values of $\alpha_M$ and $\beta_M$ at the two frequencies is $4.69 \times 10^5$ mho/cm. The best value for the conductivity of oxygen-free hard electro-formed copper at 9500 MHz is taken to be the average of the $\alpha_M$ and $\beta_M$ averages, $4.66 \times 10^5$ mho/cm. The error in this value, based on the errors in the measured values is $\pm 1.5$ percent. This value of the conductivity of copper is 80.3 percent of the dc value of copper. Previously reported values for the conductivity of copper in this frequency range, based on measurements of long lengths of waveguide operated in the propagation frequency region, vary between 85 and 78 percent of the dc conductivity.[15]

### 5.1.2 *Nickel Test Sections*

The nickel test section was made by electroplating a 0.001-inch-thick layer of commercial grade nickel on the four walls of the cutoff section of an electroformed copper test section. The wall conductivity of this copper test section was measured before plating. These results are not repeated since this measured conductivity agrees with the previously measured value of the conductivity of the copper within the error limits mentioned earlier.

The experimental measurements were made in the manner already described, at two test frequencies, 9500.873 and 9497.963 MHz. The calculated values of $\gamma l$ and the experimental points for the first test frequency is plotted in Fig. 11 as a function of conductivity. As was done for the copper measurements, two curves are plotted on the figure, one for the total real part of $\gamma l$, and one for the total imaginary part of $\gamma l$.

Figure 11 shows some interesting features of the cutoff region. The total attenuation of the nickel test section is less than that for the copper test section, indicating that the cutoff region has shifted to a lower frequency. Consistent with this shift in the cutoff region to lower frequencies is the increase in the total phase shift. However, as the conductivity is decreased below $6 \times 10^4$ mho/cm, the total attenuation increases. This result indicates that the loss resulting from the decreased conductivity is increasing faster than the cutoff region is shifting to a lower frequency by the decreasing conductivity. This difference leads to a net increase in the total loss of the cutoff section.

Only the experimental values for the first test frequency are plotted. The results at the second frequency support these results. The points

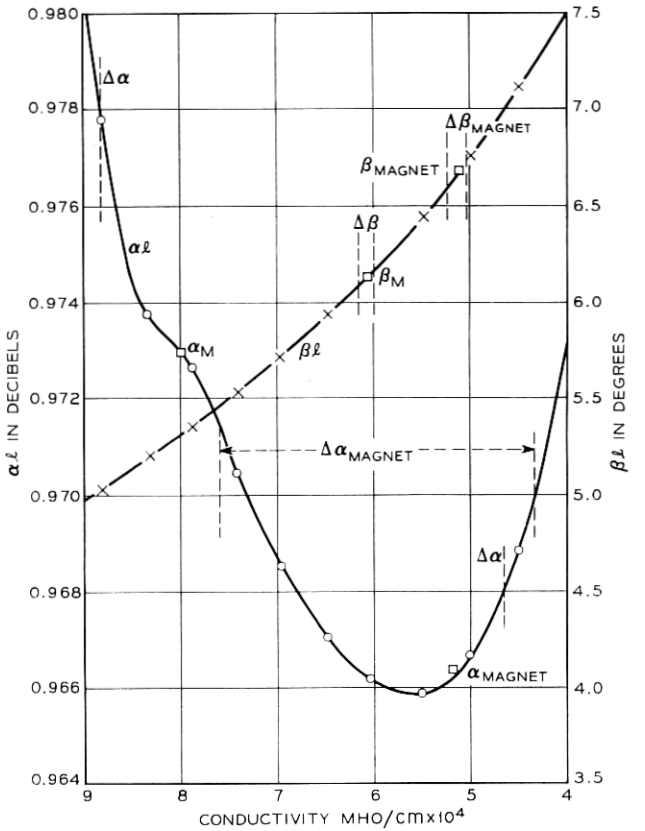


Fig. 11 — Nickel experimental results at 9500.873 MHz yielding experimental value of conductivity including effect of applied dc magnetic field. "Magnet" indicates results with magnetic field applied. ○ calculated $\alpha l$, × calculated $\beta l$, and □ measured values.

labeled $\alpha_M$ and $\beta_M$ are the experimental values. The vertical broken lines enclosing $\Delta\alpha$ and $\Delta\beta$ define the error limits in the experimental measurements. The error limits in Fig. 11 are small for the phase measurement, $\beta_M$, while the error limits for the attenuation measurement, $\alpha_M$, are large; hence the measured $\beta$ value yields the more accurate result. The figures for the copper and nickel test sections illustrate a feature of this experimental technique. At some frequency in the cutoff region both the $\alpha$ and $\beta$ measurement may have the same accuracy, while at another frequency either the $\alpha$ or $\beta$ measurement will yield a more accurate result. This feature, of course, depends on the errors in the measuring

equipment. It does allow one to choose test frequencies which will compensate for the errors in the measuring equipment.

The $\beta_M$ measurements at the two test frequencies both yield a value of $6.10 \times 10^4$ mho/cm for the conductivity of commercial grade nickel plating. The $\alpha_M$ measurements yield conductivity values of $8.0 \times 10^4$ mho and $6.4 \times 10^4$ mho/cm. However, the error limits of the $\alpha_M$ measurements include the $\beta_M$ measured values. In this case, one concludes that the most accurate measure of the conductivity of nickel is the $\beta_M$ value. The maximum range of the measured value of conductivity based on the $\beta_M$ measurement is $6.3 \times 10^4$ to $5.9 \times 10^4$ mho/cm or an error of 3.6 percent. The minimum range of the measured values is $6.0 \times 10^4$ to 6.15 mho/cm or an error of 1.7 percent.

The dc conductivity of nickel as given by various tables of the properties of metals[16] is $1.28 \times 10^5$ mho/cm. The experimentally determined value for the conductivity of nickel at 9500 GHz is $6.10 \times 10^4$ mho/cm or 47.6 per cent of the dc conductivity. The conductivity of copper at 9500 GHz was determined earlier in this paper to be 80.3 per cent of the dc value. Electroplated metals have been reported to be more porous than solid metals.[15] This increased porosity would account for the larger decrease in the conductivity of nickel compared with copper in these experiments.

The nickel plated test section was used for a second experiment. The test section was subjected to a magnetic field of 2100 gauss as discussed in Section IV. The actual field applied to the nickel was difficult to determine accurately because of the size of the Hall plate available to measure the field. It is estimated that a field of 500 gauss was applied to the nickel walls. This same field was applied to the copper test section before plating. No measurable effects were obtained.

The results of the experiment with the magnetic field are plotted in Fig. 11 as the points, $\alpha_{\text{MAGNET}}$ and $\beta_{\text{MAGNET}}$. It is evident from the location of these points on the calculated curves that the application of the magnetic field has caused an apparent decrease in the conductivity of nickel. The mean value of the conductivity resulting from the application of the magnetic field is $4.95 \times 10^4$ mho/cm.

The exact cause of this decrease in conductivity is not known. Since there was no effect of the magnetic field on the copper test section before plating, we can assume that the decrease in the conductivity of nickel resulted from the ferromagnetic properties of nickel. This effect can then be explained by assuming that the magnetic field increases the effective microwave permeability of nickel by the ratio of

6.10/4.95. The effect of the conductivity of the metal walls of a waveguide enter into the calculation of the propagation constant through the expression

$$z = \left(\frac{\omega\mu}{2\sigma}\right)^{\frac{1}{2}}.$$

Hence, the increase in the permeability, $\mu$, causes the same result as a decrease in conductivity. It is well known that nickel is ferromagnetic at low frequencies. The ferromagnetic property is described by its permeability. Evidently, if this explanation is correct, nickel exhibits a small ferromagnetic effect at microwave frequencies.

### 5.1.3 *Nichrome-Copper Test Section*

The conductivity of the walls of one of the electroformed copper type B test sections was measured and found to agree with the original copper test section within the stated error limits. Nichrome was applied to the two narrow walls as described in Section IV, and an experiment was conducted at 9497.936 MHz. The calculated values and the experimental results are plotted in Fig. 12. This figure shows the effect of conductivity on the cutoff region not present in the previous results. The $\alpha$ and $\beta$ curves have a somewhat unusual shape.

These new features are not too unusual when it is considered that we are dealing with the combination of a composite metal, nichrome over copper, on two walls of the waveguide, and a single metal, copper, on the remaining walls. The thickness of the evaporated nichrome is much less than the nichrome skin depth. The effect of this combination of metals is best understood by considering the intrinsic wall impedance defined in equation (9). The variation in this wall impedance with the change in the conductivity of the coating metal for a fixed coated metal is discussed by Ramo and Whinnery.[11]

The variation in the total attenuation as the nichrome conductivity is decreased results from two factors, the shift in the cutoff region and the increase in the skin depth of the nichrome. The rate at which these two factors change as the conductivity decreases governs the shape of the $\alpha$ and $\beta$ curves. This effect can be explained simply by considering the $\alpha$ curve. The explanation of the shape of the $\beta$ curve is more complicated and would involve repeating the analysis of Ramo and Whinnery. This is not necessary for our purposes.

As the nichrome conductivity is decreased, the skin depth of the nichrome is increased. The presence of the nichrome has less effect on

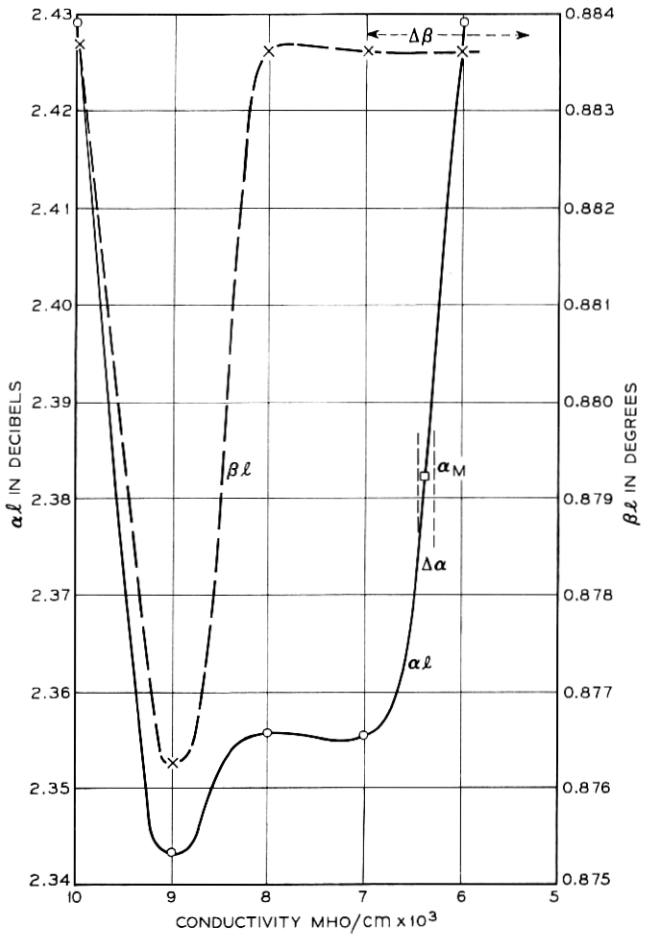


Fig. 12 — Nichrome-copper experimental results at 9497.936 MHz yielding experimental value of conductivity. ○ calculated $\alpha l$, × calculated $\beta l$, and □ measured values.

the microwave currents and the total conductivity approaches that of copper. However, until the nichrome conductivity decreases sufficiently, the conductivity of the nichrome-copper combination is less than that of copper and hence causes a shift of the cutoff region to lower frequencies with an attendant decrease in the total attenuation. As the nichrome conductivity is decreased further, the effective conductivity approaches that of copper and the cutoff region shifts to

higher frequencies. The attenuation increases again approaching that of a copper test section.

The experimental value of $\alpha$, $\alpha_M$, is plotted in Fig. 12. The experimental value of $\beta$, $\beta_M$, lies on the flat portion of the $\beta$ curve with error limits that cover the extent of the flat portion plotted. Thus the $\beta$ measurement gives no accurate measure of the conductivity of nichrome. The experimental value of nichrome conductivity at 9497 MHz based on the $\alpha$ measurement is $6.4 \times 10^3$ mho/cm. The maximum error is 1.5 percent. The dc conductivity of nichrome is $10^4$ mho/cm (See Ref. 16). The measured value of nichrome at 9497 MHz is 64 percent of the dc value.

### 5.2 *Dielectric Loaded Cutoff Test Sections*

It is well known that the insertion of a dielectric into a waveguide section causes an increase in the phase shift per unit length for frequencies above the cutoff region. The effect of lossy dielectrics placed in a waveguide section operated in the cutoff region is not well known.

Figure 13 shows the effect of a lossy dielectric in a waveguide over a frequency range covering the cutoff frequency region. The curves of the real and imaginary part of the propagation constant were plotted for several dielectric constants and loss tangents for a dielectric slab 0.059 inch thick inserted in a copper waveguide 0.62150 inch wide. The unloaded cutoff frequency of this waveguide is approximately 9500 MHz. The waveguide has a wall conductivity of $4.64 \times 10^5$ mho/cm.

Examination of these curves shows that increasing the dielectric constant for a constant loss tangent shifts the cutoff region to a lower frequency ($\alpha$ decreases, $\beta$ increases). For a constant dielectric constant an increase in the loss tangent shifts the cutoff region to a higher frequency ($\alpha$ increases, $\beta$ decreases). Although not shown in Fig. 13, a decrease in the wall conductivity of the waveguide shifts the set of curves to a lower frequency.

#### 5.2.1 *Lucite Dielectric*

The copper test section used for the original measurement of the conductivity of copper was used for the dielectric experiments. The 0.056-inch thick slab of lucite was inserted in the copper test sections.

The experimental values of $\alpha$ and $\beta$ were compared with a series of curves calculated for various combinations of dielectric constants, $\epsilon'/\epsilon_0$, and loss tangents, $\epsilon''/\epsilon_0$, for the two test frequencies, 8361.653

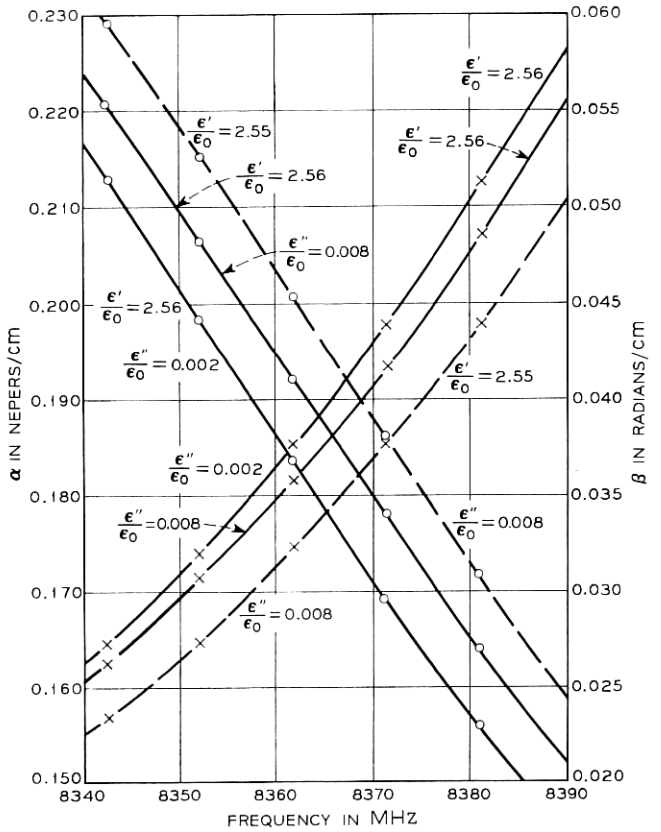


Fig. 13 — Propagation constant in cutoff region as a function of relative dielectric constant and loss tangent. ○ calculated $\alpha l$, and × calculated $\beta l$.

and 8351.945 MHz. Fig. 14 was plotted for those values which agreed with the experimental results. The results for 8351.945 MHz are not presented because they give the same result as in Fig. 14. The experimental values, $\alpha_M$ and $\beta_M$, are plotted on the respective curves of these two figures. The vertical broken lines indicate the error limits of the measured values. The curve in Fig. 14 was plotted for $\epsilon'/\epsilon_0 = 2.55$ and a range of loss tangent values, $\epsilon''/\epsilon_0$.

The error in the value of the measured $\alpha_M$ can be seen to be much less than that of $\beta_M$. This is an example of a case discussed in Section 5.1.2 where one of the parts of the propagation constant can be measured with greater accuracy than the other at the chosen frequency in the cutoff

region. From the experimental results, the experimental value of the dielectric constant of lucite is 2.55. The error limits, although not shown on the curves are 2.56 and 2.545. The measured values of the loss tangent are 0.0065 and 0.0066 giving a mean value of 0.00655. The error limits at 8361.653 MHz are 0.0064 and 0.0066; and at 8351.945 MHz, 0.0065 and 0.0067. The maximum error in the mean value of the loss tangent is 4.5 percent, and the minimum error, 1.5 percent.

The measured values of $\beta_M$ do not lie at the same values of loss tangent as those of $\alpha_M$. However, the error limits of the experimental values of $\beta_M$ enclose the error limits of the experimental values of $\alpha_M$. The measured values of $\beta_M$, while not agreeing with those of $\alpha_M$ support the more accurate values of $\alpha_M$.

The experimental values of the dielectric constant and the loss tangent

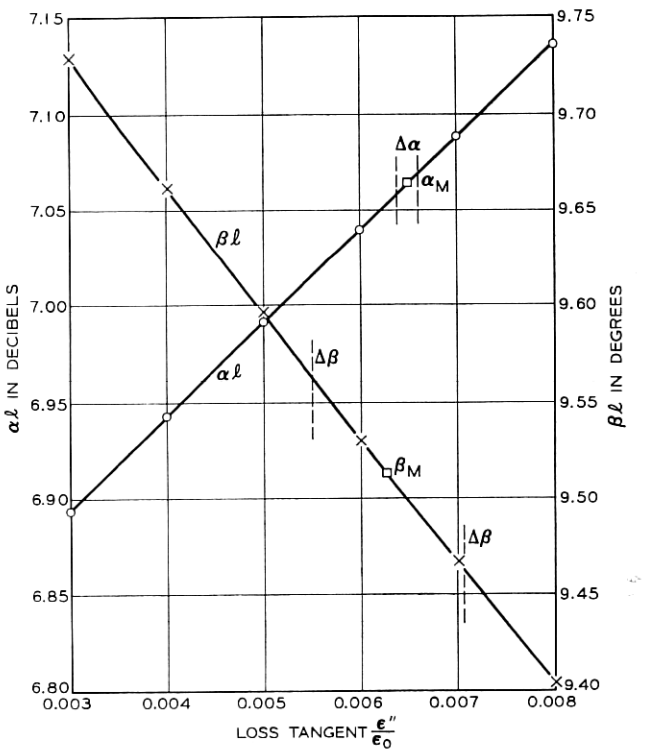


Fig. 14 — Lucite dielectric experimental results at 8361.653 MHz yielding experimental values of relative dielectric constant and loss tangent. ○ calculated $\alpha l$, × calcuated $\beta l$, and □ measured values.

for the lucite dielectric at 8350 MHz can be taken as 2.55 and 0.00655, respectively. The values reported for lucite at 10 GHz are 2.59 and 0.006, respectively.[13]

### 5.2.2 *Micarta Dielectric*

The lucite dielectric slabs in the copper test sections were replaced with 0.031-inch thick micarta slabs for an experiment in which the total attenuation and the total phase shift for various values of the dielectric constant $\epsilon'/\epsilon_0$ and the loss tangent $\epsilon''/\epsilon_0$ were calculated. The results which satisfy the experimental results are plotted in Fig. 15 for the test frequency 8477.289 MHz. Other experiments were performed at 8455.512 MHz. These experiments, although not plotted, support the results of Fig. 15.

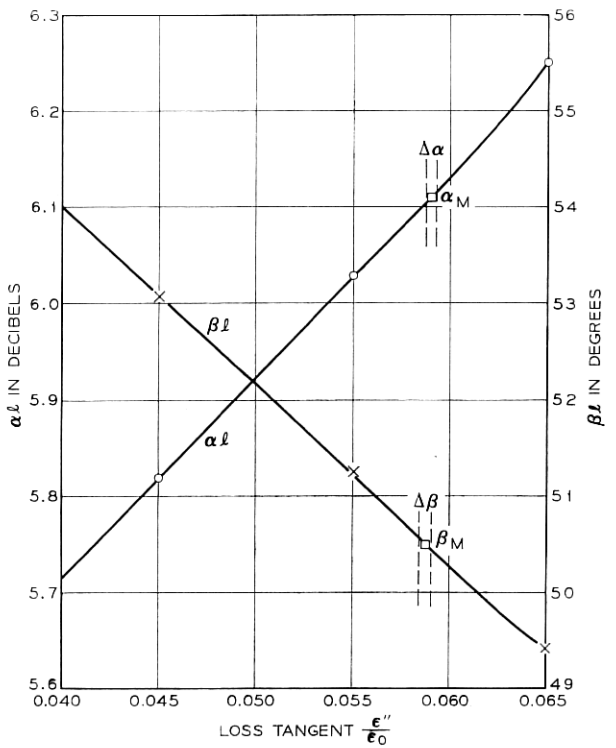


Fig. 15 — Micarta dielectric experimental results at 8477.289 MHz yielding experimental values of relative dielectric constant and loss tangent. ○ calculated $\alpha l$, × calculated $\beta l$, and □ measured values.

In these experiments with micarta, the experimental results at 8477.289 MHz yielded a dielectric constant $\epsilon'/\epsilon_0 = 3.62$, and a loss tangent based on the $\alpha$ measurement of $\epsilon''/\epsilon_0 = 0.0575$, and for the $\beta$ measurement, $\epsilon''/\epsilon_0 = 0.0580$. The results at 8455.512 MHz yielded a dielectric constant of 3.60 and a loss tangent for the $\alpha$ measurement of 0.585 and for the $\beta$ measurement of 0.0585. The mean dielectric constant, determined from the measurement at the two test frequencies, is $\epsilon'/\epsilon_0 = 3.61$ with an error of $\pm 1.5$ percent. The mean loss tangent determined from these measurements is $\epsilon''/\epsilon_0 = 0.058$ with an error of $\pm 1$ percent.

Published tables of the properties of dielectric materials list dielectric constants ranging from 3.42 to 3.78 and loss tangents ranging from 0.05 to 0.08 for micarta at 10 GHz. The range of values stems from slightly different formulations used in the manufacture of micarta. Since the definite composition of our sample of micarta is not known, it is evident that our results are quite justified.

The results discussed in the preceding sections are summarized in Table I, which lists the metal or dielectric, the frequency of measurement, the measured values of the indicated electrical properties, and the value of these properties as determined by other measurement techniques.

## VI. CONCLUSIONS

The effects of various metals and dielectrics on the properties of the cutoff region of a rectangular waveguide operated in the dominant mode have been investigated. It has been shown that a waveguide with walls of finite conductivity has a cutoff region instead of a singular cutoff frequency associated with a lossless waveguide. As the conductivity of the waveguide walls is reduced, the cutoff region is shifted to a lower frequency.

It is evident that the definition of the cutoff frequency for a lossless guide does not apply when losses are present. The definition of cutoff frequency should take into account the conductivity of the walls. The cutoff frequency for a given mode may be defined (for a given conductivity) as that frequency where the real part of the propagation constant in nepers per unit length is equal to the imaginary part of the propagation constant in radians per unit length. For the same physical dimensions, a waveguide operated in the dominant mode with walls of conductivity $\sigma_1$ would have a higher cutoff frequency than a waveguide with walls of conductivity $\sigma_2$ for $\sigma_1 > \sigma_2$.

TABLE I—MEASUREMENTS AT 72°F, 50 PERCENT RELATIVE HUMIDITY

| Metal | Measured | | Published Values* | |
|---|---|---|---|---|
| | Conductivity (mho/cm) | Frequency (MHz) | Conductivity (mho/cm) | Frequency (MHz) |
| Copper (electroformed) | $4.66 \times 10^5$ | 9500 | $5.8 \times 10^5$<br>$4.64 \times 10^5$<br>$3.15 \times 10^5$ | 0 (dc)<br>10,000<br>24,000 |
| Nickel (commercial plated) | $6.10 \times 10^4$ | 9500 | $1.28 \times 10^5$ | 0 (dc) |
| Nickel (with 800 gauss H field) | $4.95 \times 10^4$ | 9500 | None Available | |
| Nichrome (evaporated) | $6.4 \times 10^3$ | 9500 | $1.0 \times 10^4$ | 0 (dc) |

| Dielectric | Measured | | | Published Values† | | |
|---|---|---|---|---|---|---|
| | $\epsilon'/\epsilon_0$ | $\epsilon''/\epsilon_0$ | Frequency (MHz) | $\epsilon'/\epsilon_0$ | $\epsilon''/\epsilon_0$ | Frequency (MHz) |
| Lucite (sheet) | 2.55 | 0.00655 | 8350 | 2.59 | 0.006 | 10,000 |
| Micarta (sheet) | 3.61 | 0.058 | 8460 | 3.62 | 0.057 | 10,000 |

* See Refs. 6, 9, 15, and 16.
† See Refs. 9 and 13.

The introduction of a lossy dielectric into a rectangular waveguide operated in the dominant mode with walls of finite conductivity has a pronounced effect on the cutoff frequency region. A lossless dielectric inserted into a lossless waveguide produces a singular cutoff frequency at a frequency lower than that of the waveguide alone. When the waveguide walls have finite conductivity and the dielectric has a finite loss tangent, there is a cutoff region rather than a singular frequency. In this cutoff frequency region, for a constant dielectric constant, an increase in the loss tangent causes the cutoff frequency region to shift to a higher frequency. For a constant loss tangent, an increase in the dielectric constant causes the cutoff region to shift to a lower frequency. For a constant dielectric constant and loss tangent, a decrease in the wall conductivity of the waveguide causes a shift of the cutoff region to a lower frequency.

In the general case of a waveguide with walls of finite conductivity and a dielectric with a finite loss tangent, the cutoff frequency may again be defined as that frequency at which the real part of the propagation constant in nepers per unit length is equal to the imaginary part

in radians per unit length. So defined, there are generally distinct cutoff frequencies for each combination of wall conductivity, dielectric constant, loss tangent, and waveguide dimensions.

Having discussed the effect of metals and dielectrics on the cutoff region of the dominant mode of a rectangular waveguide, we turn to uses of this waveguide phenomenon. The most prominent use of the cutoff region has been examined in detail; that of measuring the properties of metals and dielectrics at microwave frequencies.

The properties of three metals, copper, nickel, and nichrome, and two dielectrics, lucite and micarta, were measured using the effect of these materials on the cutoff region. The experimental values of the metal conductivities and the relative dielectric constant and loss tangent of the dielectrics are given in Section V. The accuracy of all measured values was about $\pm 2$ per cent, although some measurements were accurate to $\pm 1$ per cent.

There are little published data on the microwave conductivity of these metals at the frequencies used for the experiments. What data are available agrees with our results to within 5 per cent. The error limits of the published values were not given; hence it is not possible to check the accuracy of the experimental values in this way.

The decrease in the conductivity of nickel in the presence of a dc magnetic field demonstrates an effect not observed in the measurements of the other metals. The exact cause of this effect is not known. It is suggested that, since nickel is ferromagnetic, the magnetic field caused a small increase in the microwave permeability of nickel. The analysis of a lossy cutoff waveguide operated at cutoff depends on the intrinsic wall impedance. Within this approximation, it is evident that an assumed increase in permeability produces the same effect as the measured decrease in the conductivity of nickel.

There are published data for lucite at 10 GHz. The values obtained from the cutoff waveguide measurements agree within 2 per cent of these values. Interpolating between the published values to obtain values for 8.5 GHz brings the agreement to about 1 per cent. The exact chemical composition of the micarta dielectric was not known. There are a range of values given in *Tables of Dielectric Properties* for different micarta compositions.[13] These published values bracket the experimental results obtained from the cutoff measurements.

Lucite was chosen as one of the test materials in order to establish a known reference to determine the total error inherent in this analysis and measurement technique. The experimental results show that the measured value of the electrical properties of lucite agree to within

1 per cent of values determined by other techniques.[13] The analysis of a lossy dielectric slab centered in a lossy waveguide operated in the cutoff frequency region requires more approximations than the analysis of the empty lossy waveguide. Hence, we would expect the maximum error to be present in the measurement of the lucite dielectric. The small error for lucite, 1 per cent, is indicative of the accuracy of this technique for measuring electrical properties of metals and dielectrics.

REFERENCES


1. Harrington, R. F., *Time Harmonic Electromagnetic Fields,* New York: McGraw-Hill, 1961.
2. Ginzton, E. L., *Microwave Measurements,* New York: McGraw-Hill, 1957.
3. Karbowiak, A. E., "Theory of Imperfect Waveguides: The Effect of Wall Impedance," Proc. IEEE (London), *102,* part B. No. 5 (September 1955), pp. 698–707.
4. Papadopoulos, V. M., "Propagation of Electromagnetic Waves in Cylindrical Waveguides with Imperfectly Conducting Walls," Quart. J. Mechanical and Applied Math. *VII,* pt. 3 (September 1954), pp. 326–334.
5. Kahn, W. K., "Power Transmission Through General Uniform Waveguides," IRE Trans. Microwave Theory and Techniques, *MTT-10,* No. 5, (September 1962), pp. 328–331.
6. Marcuvitz, N., *Waveguide Handbook,* vol. 10, Radiation Laboratory Series, New York: McGraw-Hill, 1951.
7. Barrow, W. L., "Transmission of Electromagnetic Waves in Hollow Tubes of Metal," Proc. IRE, *24,* No. 10, (October 1936), pp. 1298–1329.
8. Linder, E. G., "Attenuation of Electromagnetic Fields in Pipes Smaller than the Critical Size," Proc. IRE, *30,* No. 12 (December 1942), pp. 554–556.
9. Southworth, G. C., *Principles and Applications of Waveguide Transmission,* Princeton, N. J., D. Van Nostrand Co., 1951.
10. Montgomery, C. G., Dicke, R. H., and Purcell, E. M., *Principles of Microwave Circuits,* vol. 8, Radiation Laboratory Series, New York: McGraw-Hill, 1948.
11. Ramo, S. and Whinnery, J. R., *Fields and Waves in Modern Radio,* New York: John Wiley and Sons, Inc., 1956.
12. Adler, R. B., Chu, L. J., and Fano, R. M., *Electromagnetic Energy Transmission and Radiation,* New York: John Wiley and Sons, Inc., 1965.
13. von Hipple, A., *Tables of Dielectric Materials,* Cambridge, Mass.: Laboratory for Insulation Research, Massachusetts Institute of Technology, April 1957.
14. Cohn, S. B., and Weinhouse, N. P., "An Automatic Microwave Phase-Measurement System," Microwave J., *7,* No. 2 (February 1964), pp. 49–56.
15. E. Maxwell, "Conductivity of Metallic Surfaces," J. Appl. Phys. *18,* No. 7 (July 1947), pp. 629–638.
16. Hodgman, C. D., ed., *Handbook of Chemistry and Physics,* Cleveland, Ohio: Chemical Rubber Pub. Co., 1967.